

# CLARE: Cognitive Load Assessment in REaltime with Multimodal Data

Anubhav Bhatti, Prithila Angkan, Behnam Behinaein, Zunayed Mahmud, Dirk Rodenburg, Heather Braund, P. James Mclellan, Aaron Ruberto, Geoffery Harrison, Daryl Wilson, Adam Szulewski, Dan Howes, Ali Etemad, *Senior Member, IEEE*, Paul Hungler

**Abstract**—We present a novel multimodal dataset for Cognitive Load Assessment in REaltime (CLARE). The dataset contains physiological and gaze data from 24 participants with self-reported cognitive load scores as ground-truth labels. The dataset consists of four modalities, namely, Electrocardiography (ECG), Electrodermal Activity (EDA), Electroencephalogram (EEG), and Gaze tracking. To map diverse levels of mental load on participants during experiments, each participant completed four nine-minutes sessions on a computer-based operator performance and mental workload task (the MATB-II software) with varying levels of complexity in one minute segments. During the experiment, participants reported their cognitive load every 10 seconds. For the dataset, we also provide benchmark binary classification results with machine learning and deep learning models on two different evaluation schemes, namely, 10-fold and leave-one-subject-out (LOSO) cross-validation. Benchmark results show that for 10-fold evaluation, the convolutional neural network (CNN) based deep learning model achieves the best classification performance with ECG, EDA, and Gaze. In contrast, for LOSO, the best performance is achieved by the deep learning model with ECG, EDA, and EEG.

**Index Terms**—Multimodal Dataset, Affective Computing, Cognitive Load, ECG, EDA, EEG, GAZE .

## I. INTRODUCTION

**C**OGNITIVE LOAD assessment is an essential aspect of affective computing, defined as the amount of mental effort utilized in the working memory during performance of a task. Real-time assessment of cognitive load can enhance human-machine interactions, for instance, in training systems, education, transportation, automation, robotics, aerospace, etc. [1]–[3]. For example, quantifying the learners’ cognitive load in such training systems can lead to optimization and personalization of learning content, which in turn can lead to better and more efficient learning outcomes [4]–[7].

For cognitive load assessment, several tasks have been used to introduce varying amounts of mental workload on

participants, such as n-back tasks, visual cue tasks, games, arithmetic, multiple-choice tests, and reading exercises, [8]–[10]. One software program used for inducing varying levels of cognitive load is the Multi-Attribute Task Battery-II (MATB-II) [11]. Developed by NASA, MATB-II [11] is a computer-based program that can be used as a benchmark to evaluate the workload and performance that aircrews, under conditions similar to flight, might experience [11]. MATB-II has been widely used for assessing emotions and cognitive load in various scientific disciplines [12]–[14]. For measuring cognitive load, three general approaches are utilized: self-reporting using tools such as the National Aeronautics and Space Association Task Load Index (NASA TLX) [15] or Subjective Cognitive Load Scores (PAAS) [16], secondary behavioural performance, and the analysis of a range of physiological signals [17].

Mental workload alters sympathetic nervous system activities, which result in changes in Electrocardiogram (ECG), Electrodermal Activity (EDA), also known as Galvanic Skin Response (GSR), gaze, pupil size, Electroencephalogram (EEG), and other physiological responses. These signals can be used to estimate the cognitive load and emotional states using machine learning and deep learning algorithms [18]–[23]. Recent advances allow researchers to utilize various machine learning algorithms to classify a user’s cognitive workload using physiological measures. Despite the potential benefits and use cases of automated cognitive load measurement, the lack of annotated cognitive load datasets has been a roadblock towards creating machine learning systems capable of estimating cognitive load with high confidence. Recent studies use self-reported cognitive load as the ground truth for labelling the data; however, cognitive load is generally recorded upon completion of the experiment. This approach can affect the accuracy of the score since it is administered retrospectively, which can introduce inaccuracy due to lapses in memory and recency bias [1]. Also, rather than frequent labels captured during the performed activities, present datasets generally have a single ground truth label associated with long sequences, which can introduce further inaccuracies.

To overcome these problems, we introduce a multimodal dataset on wearable-based Cognitive Load Assessment in REaltime (CLARE). In this dataset, we collected four different data modalities, i.e., ECG, EDA, EEG, and gaze data, from 24 participants while performing MATB-II tasks designed to induce varying amounts of cognitive load. During the experiments, each participant completed four 9-minute sessions,

A. Bhatti, B. Behinaein, Z. Mahmud, P. Angkan, and A. Etemad are with the Department of Electrical and Computer Engineering and Ingenuity Research Labs, Queen’s University, Kingston, Ontario, Canada.

E-mails: anubhav.bhatti, 9hbb, zunayed.mahmud, prithila.angkan, ali.etemad@queensu.ca

D. Rodenburg, J. Mclellan, P. Hungler are with Ingenuity Research Labs, Queen’s University, Kingston, Ontario, Canada.

E-mails: d.rodenburg, james.mclellan, paul.hungler@queensu.ca

G. Harris, D. Wilson is with the Department of Psychology, Queen’s University, Kingston, Ontario, Canada.

E-mails: 8gh3@queensu.ca, daryl.wilson@queensu.ca

H. Braund, A. Ruberto, A. Szulewski, D. Howes are with the School of Medicine, Queen’s University, Kingston, Ontario, Canada.

E-mails: heather.braund, a.ruberto, adam.szulewski, d.howes@queensu.ca

TABLE I: Affect and cognitive load datasets

Dataset	Year	Subs	Affective States	Modalities	Stimuli
MAHNOB-HCI [24]	2011	27	Arousal, valence, dominance	EEG, EDA, RESP, ST, gaze, audio, video	Movie clips
DEAP [25]	2011	32	Arousal, valence, like/dislike, dominance, familiarity, face video	EEG, EOG, EMG, GSR, RESP, BVP, ST	Music video
SWELL-KW [26]	2014	25	Task load, mental effort, emotion, stress	ECG, EDA, computer logging, facial, postures	Preparing presentations, reports, email, information searching
DECAF [27]	2015	30	Arousal, valence, dominance	ECG, EMG, EOG, MEG, IR face video	Music video & videos
DREAMER [28]	2017	23	Arousal, valence, dominance	EEG, ECG	Movie clips
AMIGOS [29]	2018	40	Arousal, valence, dominance, familiarity, liking, basic emotions	ECG, EDA, EEG, audio, visual, depth (Kinect)	Videos
WESAD [30]	2018	15	Neutral, stress, amusement	<b>Chest:</b> ECG, EDA, EMG, ST, ACC, RESP; <b>Wrist:</b> EDA, BVP, ACC, ST	Trier social stress test
MPED [31]	2019	23	Joy, funny, anger, disgust, fear, sad, neutrality	ECG, EDA, EEG, RESP	Videos
CASE [32]	2019	30	Arousal, Valence	ECG, EDA, BVP, EMG, RESP, ST	Videos
CLAS [33]	2019	62	Negative emotions, mental strain, high cognitive effort	ECG, EDA, PPG, ACC	Math & logic problems, stroop test, images, audio-videos
CogLoad [8]	2020	23	Cognitive load, personality traits	EDA, ACC, ST, RR	Various cognitive load tasks
Snake [8]	2020	23	Cognitive load	EDA, ACC, ST, RR	Snake game
Kalatzis et al. [34]	2021	26	Cognitive load	ECG, RR	MATB-II
CLARE (Ours)	2022	24	Cognitive load	ECG, EDA, EEG, Gaze	MATB-II

comprised of different cognitive tasks with varying mental effort requirements. We documented the participants' self-reported subjective cognitive scores on a 9-point Likert scale at 10-second intervals during each session.

As a consequence, our dataset differs from the few cognitive load datasets that have been made publicly available. Our methodology collects subjective self-reported cognitive load scores at frequent intervals throughout the experiments, instead of the commonly used approach of retrospectively recording scores. Given its frequency, this approach better facilitates the training of supervised machine learning solutions, specifically for cognitive load assessment.

Our main contributions in this paper are as follows:

- 1) We present a new multimodal dataset on cognitive load assessment. The dataset comprises ECG (512 Hz), EDA (128 Hz), EEG (256 Hz), and Gaze tracking (50 Hz) data from 24 participants with self-reported cognitive load scores at regular intervals of 10 seconds.
- 2) We analyze and provide insights to understand the distribution of reported ground truths with respect to the complexity of performed tasks. We provide machine learning and deep learning baselines for estimating cognitive load in uni-modal and multimodal setups using two evaluation schemes, namely, 10-fold and leave-one-subject-out cross-validation.
- 3) We make the dataset publicly available to facilitate and promote realtime cognitive load estimation research and contribute to the field.

The rest of this paper is organized as follows. In Section II, we give an overview of datasets and work in affective comput-

ing and cognitive load analysis by means of biological signals. Section III explains our experimental setup and study protocol. Section IV discusses the data processing procedures and extracted features for classical machine learning algorithms. Sections V and VI present the data analysis and baseline results using the classical machine learning algorithms and deep neural network models. Finally, Section VII concludes the paper.

## II. RELATED WORK

Open datasets are crucial for conducting research, reproducing and verifying results in scientific communities. As mentioned previously, human cognitive load and affective states are interconnected and influence each other. Therefore, this section presents an overview of publicly available datasets containing biological signals for emotion recognition and cognitive load classification. Table I summarizes all the public datasets on emotion recognition and cognitive load assessment.

### A. General Affect Datasets

First, we give an overview of datasets that cover a range of affective states. MAHNOB-HCI [24] is a multimodal database containing physiological signals (ECG, EDA, RESP, ST, and EEG), facial videos, audio signals, and gaze data from 27 participants. In this dataset, movie clips were used as a stimulus for triggering affective states in participants and self-reported values of arousal, valence, and dominance were collected. Classical machine learning algorithms provided baselines for uni-modal and multimodal classification of emotions. DEAP

dataset [25] comprises a collection of biological (EEG, EOG, EMG, EDA, RESP, BVP, and ST) and facial data from 32 participants. In this experiment, the participants watched music videos that were selected to stimulate emotions. The dataset includes a self-assessment of arousal, valence, like/dislike, dominance, and familiarity. They performed baseline unimodal and multimodal classification of affect states using naive Bayes classifiers. Koldijk et al. introduced the SWELL-KW dataset [26] for investigating stress in a knowledge working environment by manipulating working conditions with stressors such as email interruptions and time pressure. SWELL-KW contains computer logging, facial expression, postures, and physiological signals (ECG and EDA) from 25 subjects. DECAF dataset [27] contains affect responses, such as valence, arousal, and dominance, of 30 subjects while watching music videos and video clips. This dataset contains ECG, EMG, EOG, magnetoencephalography (MEG), and infrared (IR) face videos. They also provide baseline scores for valence, arousal, and dominance classification using MEG signals.

A new wave of affective datasets were created and made public in 2017 and later. DREAMER [28] is a multimodal database of 23 subjects' affective states in response to movie clips. The physiological data, EEG and ECG, were captured during affect elicitation using portable, wearable, off-the-shelf wireless equipment. After each stimulus, the participants' self-assessments of their affective state valence, arousal, and dominance were recorded. They used classical machine learning to provide baselines for affect recognition using EEG and ECG. The AMIGOS dataset [29], is a multimodal dataset of affect, personality traits, and mood from 40 participants. In this dataset, affect states were elicited using short and long videos. Physiological signals (ECG, EDA, EEG), audio, and frontal HD video were recorded in this dataset. Both self-assessment of affective states (valence, arousal, dominance, familiarity, liking, and basic emotions) and external assessment of valence and arousal levels are provided in the dataset.

WESAD [30] multimodal dataset used wearable devices to collect physiological and motion data from 15 participants for stress detection. They collected data using chest-worn (ECG, EDA, EMG, ST, accelerometer (ACC), RESP) and wrist-worn (ACC, BVP, EDA, ST) sensors. The stress was elicited using Trier Social Stress Test [35] where the participants performed free speech and mental arithmetic operations in front of an audience. They recorded three different affective states, namely neutral, stress, and amusement. MPED [31], is a multimodal physiological emotion database of 23 participants. The dataset includes four physiological signals, ECG, EEG, EDA, and RESP. In this dataset, the participants watched videos that were chosen to elicit six discrete emotions. In CASE dataset [32] continuous annotation of emotions were collected from 30 participants while watching videos. The dataset included eight physiological signals (ECG, EDA, BVP, EMG, RESP, and ST) collected at a sampling rate of 1000Hz. The dataset used a joystick-based annotation method for real-time annotations of arousal and valence.

## B. Cognitive load Datasets

In this section, we review prior work that present datasets on cognitive load assessment. CLAS [33] is a multimodal dataset that collected physiological (ECG, EDA, PPG), and ACC data from 62 participants. During the experiment, to elicit emotions, mental strain, and high cognitive load, the participants performed various tasks such as solving mathematical and logical problems, taking the Stroop test, and watching images and audio-video clips. Gjoreski et al. [8] introduced two multimodal datasets, CogLoad and Snake, for facilitating research on cognitive load inference and personality traits. Both datasets collected physiological data (time interval between R-peaks (RR), EDA, ACC, and ST) from wrist-worn devices from 23 participants. In the CogLoad dataset, participants performed multiple tasks, such as 2- and 3-back tasks. In the Snake dataset, the participants played a game with varying levels of difficulty (easy, medium, and hard) on a smartphone. The participants' personality traits were recorded using questionnaires in both datasets, and their perceived cognitive load was collected using a self-reporting tool, the National Aeronautics and Space Association Task Load Index (NASA TLX) [15]. Kalatzis et al. [34] introduced a database comprising data from 26 participants for cognitive load research. ECG and RR data were collected from the participants while they performed two tasks to induce low and high cognitive workloads using the MATB-II software. The participants' perceived cognitive load levels were recorded using the NASA-TLX.

## III. EXPERIMENT SETUP

### A. MATB-II Software

To induce varying amounts of cognitive load, we used the Multi-Attribute Task Battery (MATB-II) tool [11] developed by the National Aeronautics and Space Administration (NASA)<sup>1</sup>. This tool was developed to facilitate research on human multi-task performance and mental workload. As shown in Figure 1, the MATB-II interface has five regions comprising four tasks and one scheduling region. These regions are explained as follows:

- 1) *System monitoring task*: In this task, shown as region 1 in the Figure 1, there are four slider bars (F1 to F4), and two lights (F5 that turns grey/green denoting off/on and F6 that turns grey/red for on/off). The participant's task is to reset the sliding bars when the indicator reaches either end of the bar by clicking anywhere on the bar. In secondary task, the participant needs to monitor and respond to the absence of green "light" (default state is "on"), and the presence of red "light" (default state is "off") by clicking on the respective light boxes.
- 2) *Tracking task*: In this task, shown in region 2 of Figure 1, there are two modes: automatic and manual. In the automatic mode, no attention is required from the participant, while in the manual mode, the participant needs to actively use the joystick to keep the crosshair inside the blue square in the middle.

<sup>1</sup><https://www.nasa.gov/> [Accessed: 2022-06- 05]

- 3) *Communication task*: In the communication task shown in region 3 of Figure 1, two types of audio cues play for the participants: relevant and irrelevant cues. The participant only needs to respond to the relevant cues starting with the call sign “NASA504” and ignore other call signs. Each call contains a communication channel (NAV1, NAV2, COM1, and COM2) and six digits for frequency. The participant must choose the channels for the relevant calls and subsequently enter the broadcast frequency in the frequency section.
- 4) *Resource management task*: In this task, shown in region 4 in Figure 1, the goal is to keep tanks A and B at the specified levels (marked with blue bars on the side of tanks). These tanks keep depleting during the experiment and must be refilled using tanks C, D, E, and F. The participant can circulate the fuel in the tanks using pumps marked as 1-8. The arrow ‘>’ shows the direction in which the pumps can circulate fuel. Tanks C and D have limited capacity but tanks E and F have unlimited capacity. The pumps can be toggled to ‘inactive’ (idle shown with white colour) or ‘active’ (pumping shown with green) states by clicking on them. The pumps can also break (red colour) during the experiment, making the pump unusable. After a specific time, the broken pumps are fixed automatically.
- 5) *Scheduling*: Region 5 shown in Figure 1 shows the Scheduling section where the participants can see the incoming ‘communication’ and ‘tracking’ events as a function of a vertical timeline. Event onset is signaled by arrival at the top of the timeline.

The complexity of the experiment can be modulated by changing the number of occurrences of a task or the difficulty of the tasks. For instance, the frequency of turning the green and red lights can be changed in the system monitoring task. Also, the speed of the sliders on the bars can be changed. Several parameters can be modified in the tracking task, e.g., the number of times the tracking task switches from automatic mode to manual mode and the joystick’s sensitivity and response speed. The number of relevant and irrelevant messages during an interval can be modified in the communication task. Similarly, for the resource management section, one can change the number of times the pump breaks.

We created 9 one-minute complexity levels by modifying these parameters. These mini-experiments with varying complexity levels were then arranged serially to make 9-minute sessions. One session was created in linear ‘ascending complexity’ sequence, while 8 other sessions were created by randomly concatenating the 9 levels of complexity using a Latin square approach. Each participant completed the ascending complexity experiment, followed by 3 of the 8 randomly arranged experiments. A sample of four 9-minute sessions with varying complexities is shown in Figure 4, where the first session (top-left) is the linear ascending complexity session.

### B. Ground-truth Cognitive Load Scores

For obtaining the ground-truth scores which can be used as outputs for machine learning models, we used a commonly

used 9-point Likert rating scale for cognitive load ratings as introduced in [16]. This scale ranges from very, very low mental effort (represented by 1) to very, very high mental effort (represented by 9). Participants were told to verbalize their cognitive load according to this scale at 10-second intervals. The 9-point scale is shown in Figure 3.

### C. Sensors and Placement

We recorded four modalities namely ECG, EDA, EEG, and gaze data when participants were performing the MATB-II experiments. For ECG, we used a commercially available wearable sensors, Shimmer<sup>2</sup>, with which we recorded 3-channel ECG. Sensors comprise five electrodes, of which four electrodes were attached to the clavicle and lower abdomen, and the fifth electrode was connected to the right of the sternum as a reference electrode (see Figure 2). From these five electrodes the following three signals were collected<sup>3</sup> at a sampling frequency of 512 Hz:

- 1) LA-RA: the ECG vector signal measured from the right arm (RA) position to the left arm (LA) position,
- 2) LL-RA: the ECG vector signal measured from the RA position to the left leg (LL) position,
- 3) Vx-RA: the ECG vector signal measured from the Wilson’s Central Terminal (WCT) voltage to the Vx position (in our case, sternum).

The WCT voltage is defined as an artificially constructed virtual reference potential for ECG. It is obtained by taking the average of RA, LA, and LL, and it is assumed that during the cardiac cycle it is steady with negligible amplitude [36]. These three signals were recorded and transferred by the electronic module to a laptop for storage. The electronic module was worn on the lower chest using a strap and cradle.

For EDA, we used the Shimmer EDA wearable device<sup>4</sup>. As shown in Figure 2, two sensor electrodes were attached to the index and the middle fingers of the dominant hand using electrode straps. The EDA signal was captured at a sampling frequency of 128 Hz. The electronic module was worn on the wrist of the subject using a strap. The Shimmer ECG and EDA devices are shown in figures 5a and 5b.

For collecting EEG, the Muse S Headband<sup>5</sup>, depicted in Figure 5c, was used. The device was worn on the forehead, and recorded data from four channels: AF7, AF8, TP9 and TP10<sup>6</sup>, as shown in Figure 2. Channels AF7 and AF8 collected data from the forehead, while TP9 and TP10 collected data from the back of the ears. We used an additional conductive gel to maintain better contact between the skin and the electrodes. The raw EEG signal was captured at a sampling frequency of 256 Hz.

<sup>2</sup><https://shimmersensing.com/product/consensus-bundle-development-kit/> [Accessed: 2022-05-21]

<sup>3</sup>[https://shimmersensing.com/wp-content/docs/support/documentation/ECG\\_User\\_Guide\\_Rev1.12.pdf](https://shimmersensing.com/wp-content/docs/support/documentation/ECG_User_Guide_Rev1.12.pdf) [Accessed:2022-05-21]

<sup>4</sup><https://shimmersensing.com/product/consensus-bundle-development-kit/> [Accessed: 2022-05-21]

<sup>5</sup><https://choosemuse.com/muse-s/> [Accessed: 2022-05-21]

<sup>6</sup><https://choosemuse.com/what-it-measures/> [Accessed: 2022-06-04]



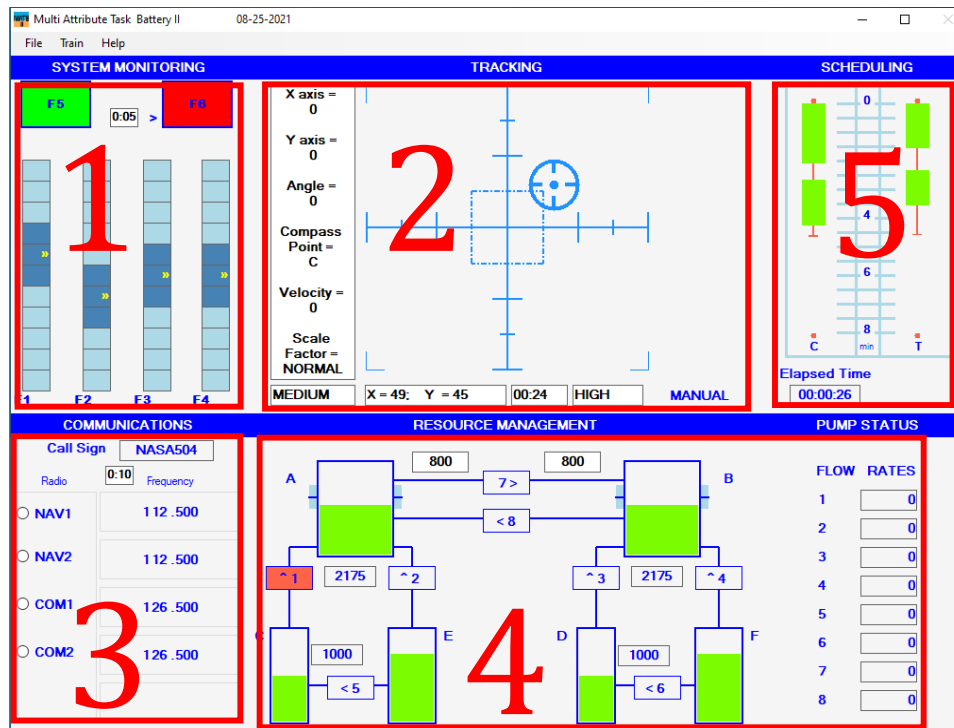


Fig. 1: A snapshot of MATB-II interface. Region 1 shows the system monitoring task, region 2 depicts the tracking task, region 3 shows the communication task, region 4 shows the resource management task, and region 5 shows the scheduler part of the software.

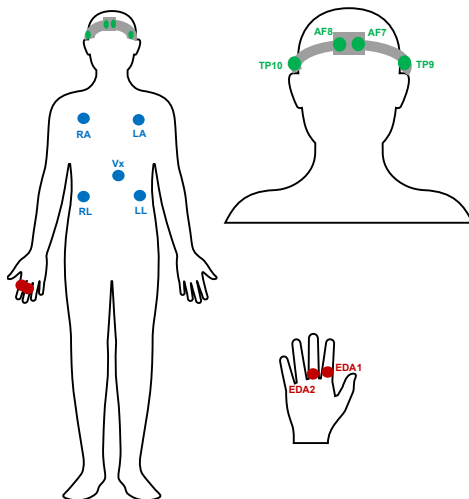


Fig. 2: Sensor placements, ECG (in blue), EDA (in red), and EEG (in green).

Finally, Tobii Pro Glasses 2<sup>7</sup>, shown in Figure 5d, were used to record the direction and velocity of the gaze. The glasses consist of two units, a head unit and a recording unit. The gaze-tracking data was recorded at a sampling rate of 50 Hz.

<sup>7</sup><https://www.tobiipro.com/product-listing/tobii-pro-glasses-2/> [Accessed: 2022-05-21]

#### D. Experiment Protocol

Ethics approval was obtained from the Queen's University Health Sciences and Affiliated Teaching Hospitals Research Ethics Board (HSREB), application number: 6025505. Participants gave informed written consent and received instructions about the experiment and the procedure 48 hours before the day of the experiment. Each participant was asked to complete a pre-participation questionnaire within 24 to 12 hours of the participation session that included several items such as quality of sleep, substance use, etc. After the arrival of each participant, members of the research team briefly explained the goal of the experiment, and introduced the participant to the different sensors. Due to the ongoing COVID-19 pandemic at the time of data collection, to maintain physical distancing, all participants placed the sensors themselves with the guidance provided by the data collection team. After the sensors were set up, participants were led to the experiment area. The experiment area comprised the following elements:

- 1) The participant desk and chair;
- 2) Computer with 27-inch Dell monitor to display MATB-II software;
- 3) Mouse and Joystick to enable participant's responses to the MATB-II tasks;
- 4) Headset (if required) to hear computer audio during the experiment;
- 5) Printed participant manual comprising cognitive load scale (1-9).

After the participant was seated, the wireless connection to the sensors was established using a remote computer (Dell

1	2	3	4	5	6	7	8	9
Very, Very Low Mental Effort	Very Low Mental Effort	Low Mental Effort	Rather Low Mental Effort	Neither Low or High Mental Effort	Rather High Mental Effort	High Mental Effort	Very High Mental Effort	Very, Very High Mental Effort

Fig. 3: Cognitive load levels on the 9-point Likert rating scale.

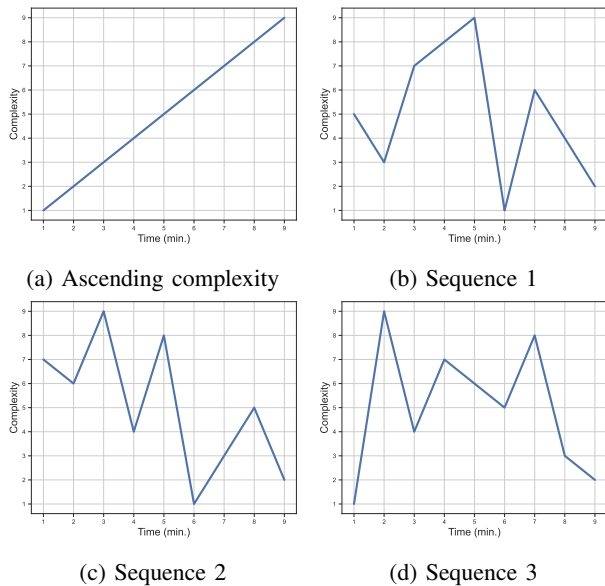


Fig. 4: Sample of complexity levels in 9-minute sessions.

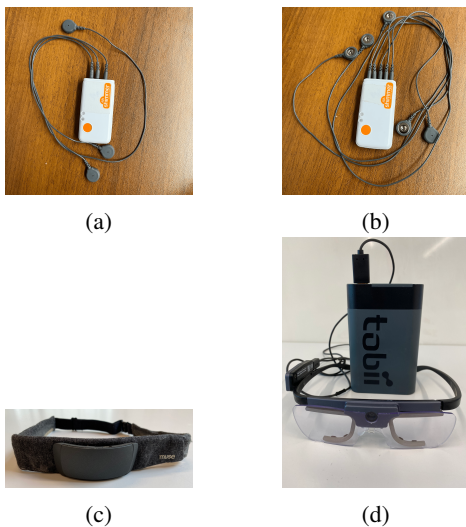


Fig. 5: (a) Shimmer ECG, (b) Shimmer EDA, (c) Muse-S band, and (d) Tobii-Pro 2 glasses

Alienware 15 laptop) for data capture via Bluetooth. An additional Bluetooth adapter was used for better connectivity and to reduce data packet loss. Then a member of the research team provided the participant with a guided walkthrough of the experiment, including the purpose of research, sequence of events, expected time commitments, and any procedural tips that could help the participant navigate the process. The layout

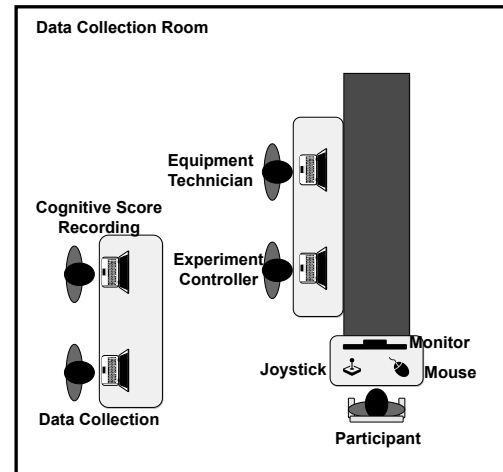


Fig. 6: Experiment setup scheme

of the experiment area is shown in Figure 6.

Subsequently, each participant went through a 1-minute practice session per task on the MATB-II, followed by another 1-minute practice session for all the tasks simultaneously. Finally, to make sure that the participants had an understanding of the low, medium, and high complexity levels, they were introduced to low, medium, and high complexity levels for another 30 seconds. After the introductory practice sessions, a 3-minute baseline was collected while the participants rested. Participants were then asked to move their eyes left and right, up and down, and blink ten times to record artifacts generated in the EEG from eye movement.

As mentioned above, each participant was asked to complete four 9-minute MATB-II sessions, the first of which was the linearly ascending complexity session. Participants provided their subjective cognitive load scores verbally during each session by responding to a beep sound after every 10-seconds. After each 9-minute session, each participant was given 2-minutes of resting time. Figure 7 shows a participant during the experiment. At the end of the fourth session, participants completed a debriefing discussion by answering some qualitative questions about the experiment. All participants received a monetary compensation of 70 CAD after the experiment.

## IV. METHOD

### A. Data Preprocessing

In this section we discuss various pre-processing steps used to filter and clean the recorded data. The raw ECG signal comprises EMG noise, powerline noise, baseline wander, and

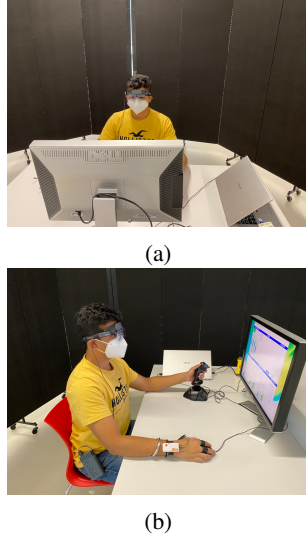


Fig. 7: (a) Experiment setup front view, and (b) experiment setup side view

T-wave interference. We applied a Butterworth bandpass filter with a passband frequency of 5-15  $Hz$  [37]. User-specific z-score normalization was applied to the filtered ECG signal [38], [39].

We removed high-frequency noise from the raw EDA signal using a lowpass filter with a cut-off frequency of 3  $Hz$ . Like ECG, we also applied user-specific z-score normalization to the filtered EDA signal. Further, a highpass filter with a cut-off frequency of 0.05  $Hz$  decomposed the filtered EDA signal into skin conductance level, also known as tonic level, and skin conductance response, also known as the phasic response [30], [39].

As mentioned in the previous section, the raw EEG signal has four channels, namely TP9, AF7, AF8, and TP10. These four channels are filtered using a Butterworth lowpass filter with a passband frequency of 0.4-128  $Hz$ . Since powerline noise frequently contaminates the EEG signal, we utilized a notch filter at 60  $Hz$  with a quality factor of 30 to remove it from each channel. Then, we performed user-specific z-score normalization to each filtered channel.

### B. Feature Extraction

After cleaning each signal, the filtered signals are divided into 10-second segments to compute various statistical and modality-specific features from each segment for modelling. A list of all features computed from ECG, EDA, EEG, and Gaze is presented in Table II, and described below.

**ECG Features:** We extracted various statistical, time domain and frequency domain features from 10-second segments of filtered ECG signals. The features included time domain features such as mean, standard deviation, maximum and minimum, and median of absolute values of HR, HRV, and filtered ECG. Additionally, skewness, kurtosis, entropy, and  $AUC^2$ , IQR, pNN20, and pNN50 were extracted. Frequency domain features were also extracted using Welch's method for power spectral analysis and included peak frequencies,

TABLE II: Extracted handcrafted affective features from each Modality for classical machine learning algorithms.

Modality	Extracted features
ECG	Time Domain Min HR, Min HRV, Min ECG, Max HR, Max HRV, Max ECG, Mean HR, Mean HRV, Mean ECG, SD HR, SD HRV, SD, ECG, RMS HRV, % HRV > 50 ms, % HRV > 20 ms, IQR HRV, IQR ECG, MAD HRV, MAD ECG, Skewness ECG, kurtosis ECG, entropy ECG, $AUC^2$ ECG
	Freq. Domain Peak frequency - ULF, VLF, LF, HF Absolute power - ULF, VLF, LF, HF Normalized power of LF & HF LF/HF ratio, Total power
EDA	Time Domain Min., Max., Mean, SD - EDA, Phasic, Tonic, Amplitude Phasic, Height Phasic, Recovery Time, Rise Time # of Peaks in Phasic IQR, MAD - EDA, Phasic, Tonic Skewness, Kurtosis, Entropy, $AUC^2$ - EDA, Phasic, Tonic
	EEG Time Domain Min., Max., Mean, Median - EEG, FFT Spectral Entropy Hjorth mobility and complexity Lempel-Ziv Complexity Higuchi fractal dimension
Gaze	Freq. Domain Min., Max., Mean, Median, Abs. Power of each Frequency Band
	Time Domain Min., Max., Mean - Pupil Diameter (Left, Right), Blink, Fixation, Fixation Dispersion, Saccade, Saccade Amplitude, Saccade Peak Velocity, Saccade Peak Acceleration, Saccade Peak Deceleration, Saccade Direction Number of Blinks, Fixations, & Saccades

absolute powers, normalized powers, and the LF/HF ratio of ultra-low frequency (ULF) band ( $< 0.003Hz$ ), very low frequency (VLF) band (0.003  $Hz$  - 0.04  $Hz$ ), low frequency (LF) band (0.04  $Hz$  - 0.15  $Hz$ ), and high frequency (HF) band (0.15  $Hz$  - 0.4  $Hz$ ), as well as the total power over all frequency bands.

**EDA Features:** As mentioned in the previous section, the filtered EDA signal is decomposed into a phasic and a tonic responses [30], [40], [41]. Statistical features, namely, minimum, maximum, mean, median, standard deviation, skewness, kurtosis, entropy, interquartile range, the squared area under the curve, median absolute deviation from EDA signal, phasic, and tonic responses, were calculated. Further, statistical features from the amplitude (excluding the tonic component), height (including the tonic component), recovery time, rise time, and the number of peaks in the phasic component are also computed.

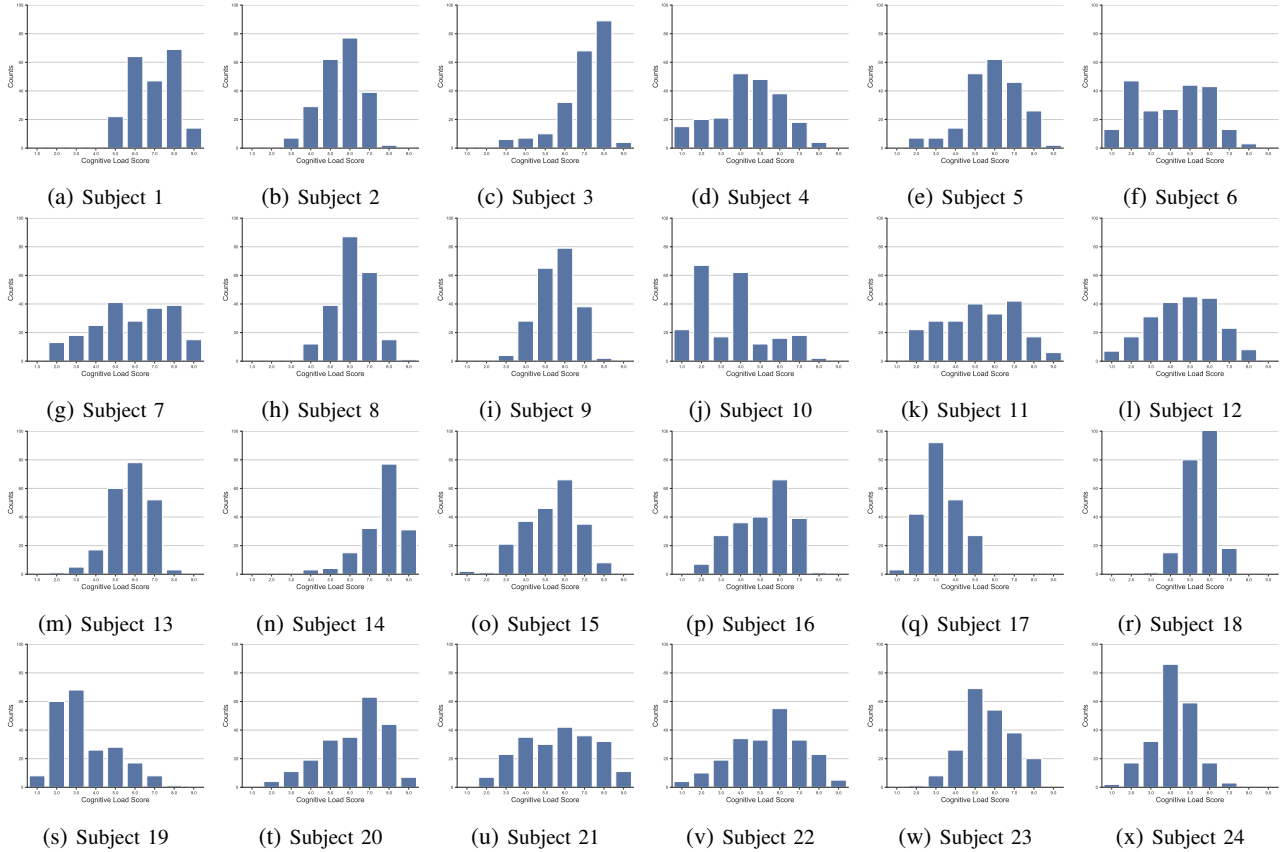


Fig. 8: Distribution of reported cognitive load values for each participant. Self-reported cognitive load levels are shown on the  $x$  axis, while  $y$  axis presents the number of times each level has been reported.

TABLE III: The architectural details (filter size, no. of filters, and stride) of the CNN network.

Block No.	Backbone Architecture with VGG Blocks
Block 1	Conv1D, 64, 32, 1 Conv1D, 64, 32, 3
Block 2	Conv1D, 32, 64, 1 Conv1D, 32, 64, 3
Block 3	Conv1D, 17, 128, 1 Conv1D, 17, 128, 3
Block 4	Conv1D, 7, 256, 1 Conv1D, 7, 256, 3
	Fully Connected, 512
	Fully Connected, 256
	SoftMax, 2

**EEG Features:** From four channels of EEG, both time and frequency domain features were computed. For each channel, features from frequency bands: Delta (0.4 - 4)  $Hz$ , Theta (4 - 8)  $Hz$ , Alpha (8 - 12)  $Hz$ , Beta (12 - 31)  $Hz$ , and Gamma (31 - 128)  $Hz$  are considered. PSD was performed on each frequency band using Welch’s method, and each frequency band’s absolute, mean, maximum, minimum, and

median power was computed. We computed spectral entropy, Hjorth mobility and complexity, Lempel-Ziv Complexity, and Higuchi fractal dimension for the time domain features for each frequency band.

**Gaze Features:** User’s gaze features such as pupillary response, blinks, eye fixation, and saccades are correlated with the cognitive load [42]–[44]. Therefore, we computed statistical features from left and right pupil diameter, blinks, fixation, and saccades. Further, we computed statistical features from saccade amplitude, velocity, acceleration, de-acceleration, and direction. We also computed the total number of blinks, fixations, and saccades.

### C. Dataset Release

To obtain access to the dataset, please contact prithila.angkan@queensu.ca

## V. DATA ANALYSIS

We examined the subjective cognitive load values recorded from each participant and compared the reported values with the complexity of the segments to better understand the distribution of the reported cognitive load scores. Figure 8 shows the distribution of the cognitive load scores reported for each individual (all sessions are combined). We see that the participants displayed a wide range of distributions, suggesting that the MATB-II software had diverse effects on the cognitive



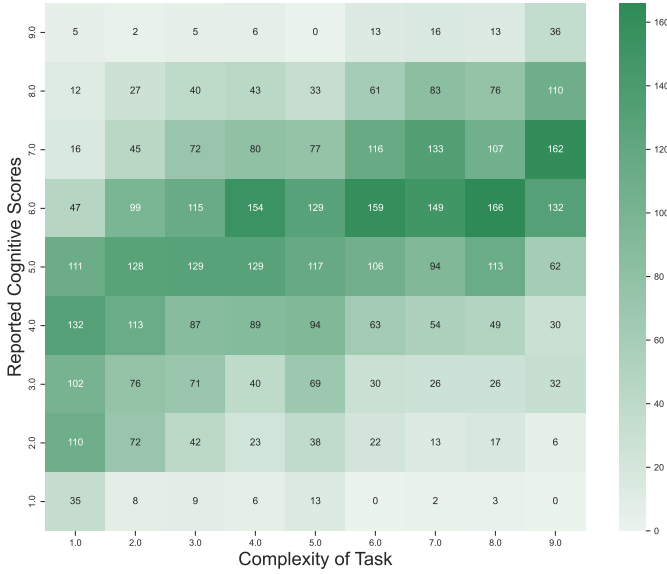


Fig. 9: Complexity vs cognitive load scores. The darker shades mean more samples.

load that the subjects felt. For example, some participants’ cognitive load ratings were on the middle or higher end of the PAAS scale (e.g., 1, 2, 3, 14). At the same time, some participants (such as 10, 17, and 19) tended to report numbers on the lower end of the spectrum. We also observed that the participants rarely reported extreme values on the scale.

We plot a heat map of complexity versus reported cognitive load scores to understand the relation between the complexity of each segment and the associated reported cognitive load values. Figure 9 shows the results of this analysis in which we observe an ‘inverted S’ relationship. From the heat map, we can see that for low complexity, most of the cognitive load values reported by participants are concentrated around 1-5; however, as the complexity of the task increases, the cognitive load values reported loosely follow the complexity values. It can also be observed from the map that for the average or higher complexity of tasks, the reported cognitive load values are concentrated between a range of 3 to 7, indicating that most participants experience moderate amounts of cognitive load when complexity is average or higher.

## VI. BENCHMARK EVALUATION

### A. Classification Algorithms

We used eight classical machine learning algorithms and a deep learning model for benchmarking. The features extracted from the four modalities in subsection IV-B served as inputs to the machine learning algorithms for classifying cognitive load scores. The eight classical machine learning algorithms are Gradient Boosting (GB), Light Gradient Boosting Machine (LGBM), Linear Discriminant Analysis (LDA), Logistic Regression (LR), Multilayer Perceptron (MLP), Random Forest (RF), Support Vector Machine (SVM), and Extreme Gradient Boosting (XGBoost). The deep learning benchmark is a VGG-style convolutional neural network (CNN).

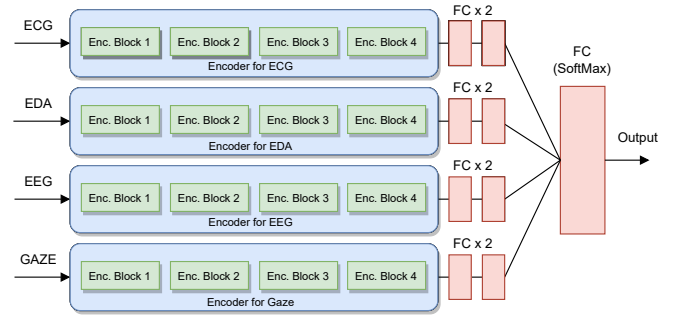


Fig. 10: A multimodal pipeline consisting of four Encoders, one for each modality.

For the GB classifier, the number of base estimators was set to 300, the loss is set to logarithmic loss, and a maximum depth of 3 was used for individual estimators. For the LGBM, the number of estimators was set to 2000, and for each base estimator, the number of leaves was set to 100. A learning rate of 0.001 was used. The ‘least squares solution’ was selected based on hyperparameter tuning for the LDA classifier. For the LR classifier, the maximum number of iterations required for the solvers to converge was set to 400, and the inverse regularization parameter ‘C’ was set to 1. The MLP classifier was trained with two hidden layers of sizes 100 and 10, and an adaptive learning rate for 1000 iterations. The number of estimators for the RF classifier was set to 1000 with a minimum sample split of 5 and a maximum depth of 5 for each tree. The SVM classifier was trained with the inverse regularization parameter ‘C’ set to 10. For the XGBoost classifier, we used a tree-based boosting method with 300 estimators. We set the learning rate and the L1 regularization values to  $1e-3$  and  $1e-4$ , respectively. The models’ parameters were tuned empirically to obtain the best training results.

VGG-like encoder blocks were used for the deep learning model, which contained two 1D convolutional layers with a ReLU activation layer and a MaxPool layer of filter size and stride of 2. The output of the fourth encoder block was fed to two FC layers with 512 and 256 units, respectively. A feature-level fusion strategy (late fusion) was then used to achieve a multimodal setup. The final output class was generated by SoftMax following an FC layer. Figure 10 shows the multimodal pipeline with the four recorded modalities. The details of filters, filter sizes, and strides for each encoder block are presented in Table III. Similar to the machine learning models, the hyperparameters of the CNN were empirically tuned to achieve the best performance.

### B. Evaluation Protocol and Implementation Details

For all the benchmarks, we use binary (‘high’ versus ‘low’) cognitive load classification. To calculate binary labels, reported scores of less than 5 were considered ‘low’ cognitive load, and scores of 5 or more were considered ‘high’ cognitive load. We use 10-fold and Leave-One-Subject-Out (LOSO) cross-validation evaluation schemes to indicate the performance of our models on previously unseen data. Accuracy and F1 score were used as evaluation metrics. For all the machine

TABLE IV: Classifiers performance for binary classification of high and low cognitive load using 10-fold evaluation scheme, the numbers are in accuracy (F1) format.

Modalities	Models								
	GB	LGBM	LDA	LR	MLP	RF	SVM	XGBoost	CNN
ECG	66.58 (65.49)	66.71 (66.27)	60.49 (57.62)	60.73 (58.21)	62.19 (61.07)	68.28 (67.38)	64.20 (63.83)	66.68 (65.26)	<b>78.45 (76.41)</b>
EDA	68.34 (67.39)	70.18 (69.64)	63.52 (61.65)	63.48 (61.53)	60.56 (59.03)	<b>71.98 (70.93)</b>	65.59 (65.00)	69.33 (68.06)	68.01 (66.21)
EEG	69.19 (68.36)	69.94 (69.42)	64.30 (63.02)	64.84 (63.62)	62.53 (61.94)	71.85 (71.02)	69.09 (68.67)	69.91 (69.00)	<b>74.10 (72.08)</b>
Gaze	66.85 (66.01)	67.97 (67.45)	62.39 (60.11)	62.50 (60.35)	61.54 (59.61)	<b>69.70 (68.66)</b>	65.83 (65.51)	67.80 (66.72)	66.78 (64.23)
ECG, EDA	70.08 (69.31)	71.98 (71.56)	64.37 (62.89)	64.67 (63.20)	59.95 (58.15)	73.24 (72.51)	69.30 (68.83)	70.96 (70.15)	<b>79.72 (77.53)</b>
ECG, EEG	70.76 (69.99)	70.18 (69.67)	65.66 (64.59)	65.93 (64.96)	63.38 (62.56)	72.53 (71.77)	68.75 (68.33)	69.30 (68.32)	<b>77.66 (75.77)</b>
ECG, Gaze	68.96 (68.11)	70.38 (69.92)	63.96 (62.71)	64.13 (62.92)	63.86 (62.67)	71.00 (70.06)	67.80 (67.33)	70.59 (69.71)	<b>78.41 (76.54)</b>
EDA, EEG	72.19 (71.39)	72.09 (71.63)	65.35 (64.21)	65.28 (64.22)	60.96 (59.17)	73.61 (72.85)	68.86 (68.40)	72.49 (71.65)	<b>75.30 (73.45)</b>
EDA, Gaze	71.34 (70.63)	72.32 (71.87)	65.45 (64.12)	65.73 (64.43)	57.67 (54.13)	<b>74.40 (73.65)</b>	68.85 (68.34)	72.63 (71.83)	70.64 (68.23)
EEG, Gaze	71.64 (70.92)	71.71 (71.21)	66.98 (66.08)	67.43 (66.48)	66.30 (64.85)	73.65 (72.76)	70.79 (70.40)	71.40 (70.59)	<b>75.50 (73.13)</b>
ECG, EDA, EEG	71.10 (70.42)	72.90 (72.57)	66.13 (65.07)	65.73 (64.74)	61.71 (60.51)	73.65 (72.97)	69.87 (69.43)	72.53 (71.72)	<b>80.10 (78.49)</b>
ECG, EDA, Gaze	72.12 (71.45)	73.24 (72.86)	67.12 (66.04)	66.61 (65.60)	62.39 (60.10)	74.53 (73.85)	70.96 (70.49)	73.27 (72.54)	<b>80.30 (78.34)</b>
ECG, EEG, Gaze	71.51 (70.82)	72.80 (72.34)	67.56 (66.74)	68.51 (67.67)	66.54 (65.14)	74.09 (73.26)	71.13 (70.80)	71.64 (70.85)	<b>78.26 (76.56)</b>
EDA, EEG, Gaze	73.58 (72.96)	73.58 (73.13)	67.97 (67.13)	67.87 (67.03)	61.51 (59.51)	75.18 (74.45)	71.71 (71.26)	74.50 (73.78)	<b>75.87 (74.08)</b>
All modalities	73.38 (72.81)	74.26 (73.83)	68.24 (67.47)	68.38 (67.59)	62.36 (60.66)	75.14 (74.47)	72.05 (71.59)	74.26 (73.60)	<b>79.65 (77.94)</b>

TABLE V: Classifiers performance for binary classification of high and low cognitive load using leave-one-subject-out evaluation scheme, the numbers are in accuracy (F1) format.

Modalities	Models								
	GB	LGBM	LDA	LR	MLP	RF	SVM	XGBoost	CNN
ECG	53.23 (45.21)	42.00 (33.06)	55.60 (43.79)	43.34 (35.22)	43.15 (39.08)	55.60 (44.16)	40.26 (33.09)	40.00 (28.79)	<b>63.28 (51.00)</b>
EDA	58.67 (50.86)	55.20 (51.03)	60.15 (51.23)	50.81 (47.56)	48.90 (43.91)	59.36 (49.50)	50.46 (47.42)	51.52 (47.67)	<b>64.08 (54.80)</b>
EEG	54.71 (47.06)	53.35 (46.40)	49.76 (43.83)	52.38 (44.16)	54.46 (48.94)	59.17 (46.57)	53.23 (47.03)	56.54 (48.95)	<b>65.21 (52.15)</b>
Gaze	54.61 (47.35)	54.79 (46.41)	56.72 (42.49)	52.79 (43.97)	53.08 (44.76)	58.80 (48.83)	51.63 (44.05)	56.93 (46.53)	<b>60.23 (52.92)</b>
ECG, EDA	58.66 (50.54)	45.88 (38.04)	58.37 (47.25)	51.87 (48.68)	47.60 (44.53)	62.23 (51.60)	50.58 (47.58)	47.50 (43.31)	<b>64.48 (55.38)</b>
ECG, EEG	55.10 (48.49)	53.54 (46.77)	50.27 (44.37)	51.97 (44.11)	52.17 (47.11)	56.32 (43.89)	49.29 (43.36)	56.97 (50.15)	<b>65.22 (51.00)</b>
ECG, Gaze	54.29 (49.07)	56.62 (50.75)	57.21 (47.22)	57.22 (47.42)	53.65 (48.40)	57.66 (47.21)	54.51 (47.36)	56.59 (49.79)	<b>59.27 (50.81)</b>
EDA, EEG	56.53 (49.60)	57.91 (52.19)	51.51 (44.89)	51.27 (44.51)	52.80 (46.45)	60.33 (48.58)	53.19 (47.38)	62.30 (54.40)	<b>65.94 (56.46)</b>
EDA, Gaze	59.74 (54.60)	60.80 (53.98)	58.28 (49.39)	57.55 (48.64)	54.12 (47.70)	63.88 (53.86)	56.23 (49.43)	62.29 (55.87)	<b>63.95 (56.89)</b>
EEG, Gaze	60.63 (53.31)	60.01 (53.18)	57.74 (48.44)	57.57 (49.15)	58.90 (49.53)	<b>61.41 (48.68)</b>	57.50 (49.98)	60.22 (52.86)	60.90 (52.04)
ECG, EDA, EEG	58.34 (51.06)	59.96 (52.88)	52.00 (45.33)	50.72 (44.10)	53.38 (47.55)	60.54 (48.45)	53.48 (46.50)	61.66 (54.38)	<b>65.48 (55.72)</b>
ECG, EDA, Gaze	59.79 (52.34)	60.47 (54.12)	57.20 (47.83)	56.51 (47.48)	58.71 (49.91)	<b>63.02 (51.48)</b>	58.05 (51.30)	61.04 (54.06)	62.08 (55.10)
ECG, EEG, Gaze	58.54 (51.16)	58.37 (52.30)	57.63 (49.93)	57.74 (50.91)	56.78 (48.50)	60.34 (47.60)	54.73 (47.46)	59.99 (53.31)	<b>60.97 (51.51)</b>
EDA, EEG, Gaze	61.90 (54.95)	61.55 (55.55)	56.63 (48.09)	56.38 (48.92)	52.31 (45.70)	62.25 (50.91)	58.42 (50.96)	61.95 (55.68)	<b>63.65 (56.13)</b>
All modalities	57.95 (51.58)	<b>63.91 (56.59)</b>	56.35 (50.52)	54.72 (49.67)	54.89 (48.94)	62.73 (51.58)	58.63 (50.49)	63.75 (56.95)	61.38 (55.34)

learning algorithms except LGBM and XGBoost, we use the Scikit-learn<sup>8</sup> library. All the parameters of the machine learning algorithms were optimized by performing an exhaustive search. Our deep learning pipelines were implemented using the TensorFlow framework. For the CNN, we used AdaDelta with a decay rate of 0.95, a learning rate of 5e-3, and focal loss (alpha of 4.0 and gamma of 2.0). We empirically selected a batch size of 256 for 100 epochs for all experiments. We implemented our pipelines using an Intel Core i7-9700 CPU and an NVIDIA GeForce RTX 2080 Ti GPU.

### C. Results

This section provides the uni-modal, and multimodal benchmark binary classification results from machine learning and the deep learning classifiers with two evaluation schemes, namely 10-fold and the LOSO evaluation scheme. The benchmark results for 10-fold and LOSO schemes are provided in

Table IV and V, respectively. Below we discuss these results in detail.

1) *10-Fold Cross Validation*: In this evaluation scheme, we observe that the CNN generally has the best (accuracy = 80.30, F1 = 78.34 with ECG, EDA, and GAZE) and the most consistent performance for both accuracy and F1. This is followed by the RF classifier (accuracy = 75.18, F1 = 74.45 with EDA, EEG, and Gaze), which in some cases, outperforms the CNN (e.g., for EDA and/or Gaze). In terms of individual modalities, it can be seen the ECG is the most important, with which the uni-modal classification accuracy and F1 are 78.45 and 76.41, respectively. In the bi-modal setup, we observe that ECG and EDA show the highest results (accuracy = 79.72, F1 = 77.53), followed by ECG and Gaze (accuracy = 78.41, F1 = 76.54). The highest results for tri-modal learning are achieved with ECG, EDA, and Gaze (accuracy = 80.30, F1 = 78.34), closely followed by ECG, EDA, and EEG (accuracy = 80.10, F1 = 78.49). Interestingly, when compared to tri-modal learning results, the performance of the classifiers decreases

<sup>8</sup><https://scikit-learn.org/stable/>

when all four modalities are used.

2) *LOSO Cross Validation*: As the leave-one-subject-out cross-validation evaluation scheme is more challenging than the 10-fold scheme, the performance of classical machine learning and deep learning models decrease in comparison to the 10-fold evaluation scheme. Consistent with our observations for 10-fold evaluation, we observe that for LOSO, CNN has the best performance (accuracy = 65.94, F1 = 56.46), followed by the RF, XGBoost, and LGBM classifier. In some cases, the RF classifier (EEG & Gaze, and ECG, EDA & Gaze) and the LGBM classifier (all modalities) outperform the CNN. In terms of individual modalities, we observe that EEG is the most important modality and yields the best results with accuracy and F1 of 65.21 and 52.15, respectively. Following the same trend, for bi-modal learning, the best results are achieved using EDA and EEG (accuracy = 65.94, F1 = 56.46) followed by ECG and EEG (accuracy = 65.22, F1 = 51.00). The best results for tri-modal learning are achieved with ECG, EDA, and EEG (accuracy = 65.48, F1 = 55.72). When all four modalities (ECG, EDA, EEG, and Gaze) are combined, the best results are achieved with LGBM (accuracy = 63.91, F1 = 56.59).

#### D. Inference Time

As mentioned earlier, in this experiment, the ground truth labels were recorded at 10-second intervals to facilitate the collection of the frequent ground truth labels. This allows for better estimation of cognitive load scores by machine learning models. To meet the real-time inference requirements, the model constraint would be to generate the output prediction in less time than the ground truth collection interval. For classical machine learning models, the inference time would depend on the time to compute handcrafted features and the time to make a prediction. In contrast, for the deep learning model, as there is no computation of handcrafted features, the inference time would depend on the time taken to make a prediction. So, we extract low complexity features for classical machine learning models [45]. Given the number of handcrafted features from four modalities, the average time to compute these features for one sample was approximately 1 second. We then evaluated and present the average inference time of each classical machine learning model and deep learning model in Table VI. The table shows that RF, XGBoost, and CNN models take significantly more time than the other methods; however, the inference time is still under 1 second for all the algorithms that satisfy the real-time inference requirements.

#### VII. CONCLUSION AND FUTURE DIRECTIONS

In summary, we collected a new multimodal dataset, CLARE, with self-reported *cognitive load* as ground-truth labels. The dataset comprised four modalities (ECG, EDA, EEG, and Gaze) from 24 participants. We used MATB-II software to develop nine different complexity levels, each with a duration of 1 minute, to induce varying levels of mental load on participants. Each participant completed four separate sessions comprising nine randomly selected 1-minute segments. They reported their subjective cognitive load every

TABLE VI: Average Inference Time

Classifiers	Inference Time ( $\mu$ s)
Gradient Boosting	20.99
Light Gradient Boosting Machine	64.17
Linear Discriminant Analysis	15.97
Logistic Regression	16.47
Multi-Layer Perceptron	20.52
Random Forest	605.88
Support Vector Machine	446.64
Extreme Gradient Boosting	1482.30
CNN	4519.99

10 seconds during the experiment as physiological signals were recorded. To evaluate our dataset, we provide uni-modal and multimodal benchmarks from machine learning and deep learning classifiers with a 10-fold and leave-one-subject-out evaluation scheme.

We identify a few limitations and future directions for the dataset collection and design. As explained earlier, participants were asked to report their cognitive load score at 10-second intervals during the experiments. While this design intended for frequent ground-truth labels to be recorded, which would benefit machine learning models, it may have induced an additional unwanted cognitive load on the participants. For future similar data collection protocols, studies can be done to identify the optimum balance between the frequency of collected labels and the added distraction caused by the collection effort. Such a study can inform more optimized protocols for cognitive load and affective computing studies.

The experiment results suggest that the accurate, real time evaluation and presentation of cognitive load is possible and that the outputs can potentially be used to support cognitive performance in a broad range of contexts. The results also suggest that in terms of number of signals/modalities “more is not always better” and accurately indexing cognitive load can be accomplished with a carefully selected subset of physiological signals.

#### VIII. ACKNOWLEDGEMENT

We would like to thank the Innovation for Defence Excellence and Security (IDEaS) program under the Department of National Defence (DND) for funding this project.

#### REFERENCES

- [1] R. McKendrick, B. Feest, A. Harwood, and B. Falcone, “Theories and methods for labeling cognitive workload: Classification and transfer learning,” *Frontiers in Human Neuroscience*, vol. 13, p. 295, 2019. 1
- [2] L. Fridman, B. Reimer, B. Mehler, and W. T. Freeman, “Cognitive load estimation in the wild,” in *Proceedings of the 2018 CHI Conference on Human Factors in Computing Systems*, 2018, pp. 1–9. 1
- [3] M. I. Ahmad, I. Keller, D. A. Robb, and K. S. Lohan, “A framework to estimate cognitive load using physiological data,” *Personal and Ubiquitous Computing*, pp. 1–15, 2020. 1
- [4] R. Brünken, T. Seufert, and F. Paas, “Measuring cognitive load,” *Cognitive load theory*, pp. 181–202, 2010. 1
- [5] K. H. Teigen, “Yerkes-dodson: A law for all seasons,” *Theory & Psychology*, vol. 4, no. 4, pp. 525–547, 1994. 1
- [6] J. Sweller, “Cognitive load theory, learning difficulty, and instructional design,” *Learning and instruction*, vol. 4, no. 4, pp. 295–312, 1994. 1

- [7] A. Szulewski, D. Howes, J. J. van Merriënboer, and J. Sweller, "From theory to practice: the application of cognitive load theory to the practice of medicine," *Academic Medicine*, vol. 96, no. 1, pp. 24–30, 2020. **1**
- [8] M. Gjoreski, T. Kolenik, T. Knez, M. Luštrek, M. Gams, H. Gjoreski, and V. Pejović, "Datasets for cognitive load inference using wearable sensors and psychological traits," *Applied Sciences*, vol. 10, no. 11, p. 3843, 2020. **1, 2, 3**
- [9] I. Mijić, M. Šarlija, and D. Petrinović, "Mmod-cog: A database for multimodal cognitive load classification," in *2019 11th International Symposium on Image and Signal Processing and Analysis (ISPA)*. IEEE, 2019, pp. 15–20. **1**
- [10] A. Szulewski, N. Roth, and D. Howes, "The use of task-evoked pupillary response as an objective measure of cognitive load in novices and trained physicians: a new tool for the assessment of expertise," *Academic Medicine*, vol. 90, no. 7, pp. 981–987, 2015. **1**
- [11] Y. Santiago-Espada, R. R. Myer, K. A. Latorella, and J. R. Comstock Jr, "The multi-attribute task battery ii (MATB-II) software for human performance and workload research: A user's guide," 2011. **1, 3**
- [12] L. Kennedy and S. H. Parker, "Making matb-ii medical: pilot testing results to determine a novel lab-based, stress-inducing task," in *Proceedings of the international symposium on human factors and ergonomics in health care*, vol. 6, no. 1. SAGE Publications Sage CA: Los Angeles, CA, 2017, pp. 201–208. **1**
- [13] S. Chandra, G. Sharma, K. Verma, A. Mittal, and D. Jha, "EEG based cognitive workload classification during NASA MATB-II multitasking," *International Journal of Cognitive Research in Science, Engineering and Education*, vol. 3, no. 1, 2015. **1**
- [14] H. Qu, X. Gao, and L. Pang, "Classification of mental workload based on multiple features of ECG signals," *Informatics in Medicine Unlocked*, vol. 24, p. 100575, 2021. **1**
- [15] S. G. Hart and L. E. Staveland, "Development of NASA-TLX (Task Load Index): Results of empirical and theoretical research," in *Advances in Psychology*. Elsevier, 1988, vol. 52, pp. 139–183. **1, 3**
- [16] F. G. Paas, "Training strategies for attaining transfer of problem-solving skill in statistics: a cognitive-load approach," *Journal of educational psychology*, vol. 84, no. 4, p. 429, 1992. **1, 4**
- [17] F. Paas, J. E. Tuovinen, H. Tabbers, and P. W. Van Gerven, "Cognitive load measurement as a means to advance cognitive load theory," in *Educational psychologist*. Routledge, 2016, pp. 63–71. **1**
- [18] K. Ross, P. Sarkar, D. Rodenburg, A. Ruberto, P. Hungler, A. Szulewski, D. Howes, and A. Etemad, "Toward dynamically adaptive simulation: Multimodal classification of user expertise using wearable devices," *Sensors*, vol. 19, no. 19, p. 4270, 2019. **1**
- [19] P. Antonenko, F. Paas, R. Grabner, and T. Van Gog, "Using electroencephalography to measure cognitive load," *Educational Psychology Review*, vol. 22, no. 4, pp. 425–438, 2010. **1**
- [20] L. Perkhofer and O. Lehner, "Using gaze behavior to measure cognitive load," in *Information Systems and Neuroscience*. Springer, 2019, pp. 73–83. **1**
- [21] K. Krejtz, A. T. Duchowski, A. Niedzielska, C. Biele, and I. Krejtz, "Eye tracking cognitive load using pupil diameter and microsaccades with fixed gaze," *PLoS One*, vol. 13, no. 9, p. e0203629, 2018. **1**
- [22] A. Bhatti, B. Behinaein, P. Hungler, and A. Etemad, "Attx: Attentive cross-connections for fusion of wearable signals in emotion recognition," *arXiv preprint arXiv:2206.04625*, 2022. **1**
- [23] P. Sarkar, A. Posen, and A. Etemad, "Avcaff: A large scale audio-visual dataset of cognitive load and affect for remote work," in *Proceedings of the AAAI Conference on Artificial Intelligence*, vol. 37, no. 1, 2023, pp. 76–85. **1**
- [24] M. Soleymani, J. Lichtenauer, T. Pun, and M. Pantic, "A multimodal database for affect recognition and implicit tagging," *IEEE transactions on affective computing*, vol. 3, no. 1, pp. 42–55, 2011. **2**
- [25] S. Koelstra, C. Muhl, M. Soleymani, J.-S. Lee, A. Yazdani, T. Ebrahimi, T. Pun, A. Nijholt, and I. Patras, "Deap: A database for emotion analysis; using physiological signals," *IEEE Transactions On Affective Computing*, vol. 3, no. 1, pp. 18–31, 2011. **2, 3**
- [26] S. Koldijk, M. Sappelli, S. Verberne, M. A. Neerinx, and W. Kraaij, "The SWELL knowledge work dataset for stress and user modeling research," in *Proceedings of the 16th International Conference on Multimodal Interaction*, 2014, pp. 291–298. **2, 3**
- [27] M. K. Abadi, R. Subramanian, S. M. Kia, P. Avesani, I. Patras, and N. Sebe, "DECAF: MEG-based multimodal database for decoding affective physiological responses," *IEEE Transactions on Affective Computing*, vol. 6, no. 3, pp. 209–222, 2015. **2, 3**
- [28] S. Katsigiannis and N. Ramzan, "Dreamer: A database for emotion recognition through EEG and ECG signals from wireless low-cost off-the-shelf devices," *IEEE Journal Of Biomedical And Health Informatics*, vol. 22, no. 1, pp. 98–107, 2017. **2, 3**
- [29] J. A. M. Correa, M. K. Abadi, N. Sebe, and I. Patras, "Amigos: A dataset for affect, personality and mood research on individuals and groups," *IEEE Transactions on Affective Computing*, 2018. **2, 3**
- [30] P. Schmidt, A. Reiss, R. Duerichen, C. Marberger, and K. Van Laerhoven, "Introducing WESAD, a multimodal dataset for wearable stress and affect detection," in *Proceedings of the 20th ACM International Conference on Multimodal Interaction*, 2018, pp. 400–408. **2, 3, 7**
- [31] T. Song, W. Zheng, C. Lu, Y. Zong, X. Zhang, and Z. Cui, "MPED: A multi-modal physiological emotion database for discrete emotion recognition," *IEEE Access*, vol. 7, pp. 12 177–12 191, 2019. **2, 3**
- [32] K. Sharma, C. Castellini, E. L. van den Broek, A. Albu-Schaeffer, and F. Schwenker, "A dataset of continuous affect annotations and physiological signals for emotion analysis," *Scientific data*, vol. 6, no. 1, pp. 1–13, 2019. **2, 3**
- [33] V. Markova, T. Ganchev, and K. Kalinkov, "Clas: a database for cognitive load, affect and stress recognition," in *2019 International Conference on Biomedical Innovations and Applications (BIA)*. IEEE, 2019, pp. 1–4. **2, 3**
- [34] A. Kalatzis, A. Teotia, V. G. Prabhu, and L. Stanley, "A database for cognitive workload classification using electrocardiogram and respiration signal," in *International Conference on Applied Human Factors and Ergonomics*. Springer, 2021, pp. 509–516. **2, 3**
- [35] C. Kirschbaum, K.-M. Pirke, and D. H. Hellhammer, "The 'Trier Social Stress Test' – a tool for investigating psychobiological stress responses in a laboratory setting," *Neuropsychobiology*, vol. 28, no. 1-2, pp. 76–81, 1993. **3**
- [36] H. Moeinzadeh, G. Gargiulo, P. Bifulco, M. Cesarelli, A. O'Loughlin, M. Shugman, and A. Thiagalingam, "A modern wilson's central terminal electrocardiography database," *Heart, Lung and Circulation*, vol. 27, pp. S293–S294, 2018. **4**
- [37] J. Pan and W. J. Tompkins, "A real-time QRS detection algorithm," *IEEE Transactions on Biomedical Engineering*, no. 3, pp. 230–236, 1985. **7**
- [38] B. Behinaein, A. Bhatti, D. Rodenburg, P. Hungler, and A. Etemad, "A transformer architecture for stress detection from ecg," in *2021 International Symposium on Wearable Computers*, 2021, pp. 132–134. **7**
- [39] A. Bhatti, B. Behinaein, D. Rodenburg, P. Hungler, and A. Etemad, "Attentive cross-modal connections for deep multimodal wearable-based emotion recognition," in *2021 9th International Conference on Affective Computing and Intelligent Interaction Workshops and Demos (ACIIW)*. IEEE, 2021, pp. 01–05. **7**
- [40] J. Choi, B. Ahmed, and R. Gutierrez-Osuna, "Development and evaluation of an ambulatory stress monitor based on wearable sensors," *IEEE transactions on information technology in biomedicine*, vol. 16, no. 2, pp. 279–286, 2011. **7**
- [41] J. A. Healey and R. W. Picard, "Detecting stress during real-world driving tasks using physiological sensors," *IEEE Transactions on intelligent transportation systems*, vol. 6, no. 2, pp. 156–166, 2005. **7**
- [42] A. F. Kramer, "Physiological metrics of mental workload: A review of recent progress," *Multiple-task performance*, pp. 279–328, 2020. **8**
- [43] J. Zagermann, U. Pfeil, and H. Reiterer, "Measuring cognitive load using eye tracking technology in visual computing," in *Proceedings of the sixth workshop on beyond time and errors on novel evaluation methods for visualization*, 2016, pp. 78–85. **8**
- [44] S. Chen, J. Epps, N. Ruiz, and F. Chen, "Eye activity as a measure of human mental effort in hci," in *Proceedings of the 16th international conference on Intelligent user interfaces*, 2011, pp. 315–318. **8**
- [45] C. Loconsole, D. Chiaradia, V. Bevilacqua, and A. Frisoli, "Real-time emotion recognition: an improved hybrid approach for classification performance," in *Intelligent Computing Theory: 10th International Conference, ICIC 2014, Taiyuan, China, August 3-6. Proceedings 10*. Springer, 2014, pp. 320–331. **11**